Error Characteristics of GPS RO Atmospheric Profiles

B. Scherllin-Pirscher (1,2,3), A. K. Steiner (1), U. Foelsche (1), G. Kirchengast (1), Y.-H. Kuo (2)

(1) Wegener Center for Climate and Global Change (WegCenter) and Institute for Geophysics, Astrophysics, and Meteorology/Institute for Physics, University of Graz, Graz, Austria
(2) COSMIC Project Office, University Corporation for Atmospheric Research, Boulder, Colorado, USA
(3) Advanced Study Program, National Center for Atmospheric Research, Boulder, Colorado, USA

INTRODUCTION

In the upper troposphere and lower stratosphere (UTLS) region the radio occultation (RO) technique (Figure 1) provides accurate profiles of atmospheric parameters. These profiles can be used in operational meteorology (i.e., numerical weather prediction), atmospheric and climate research. At the Wegener Center for Climate and Global Change (WEGC), University of Graz, an RO retrieval scheme has been established, which uses phase delay profiles and precise orbit information provided by other data centers and computes atmospheric profiles of bending angle BA, refractivity N, dry pressure p_{dry}, dry geopotential height Z_{dry}, and dry temperature T_{dry}. We present the quality and observational errors of RO data retrieved with the current retrieval version OPSv5.4 and compare characteristics of CHAMP, GRACE-A, FORMOSAT-3/COSMIC (F3C), and MetOp/GRAS.

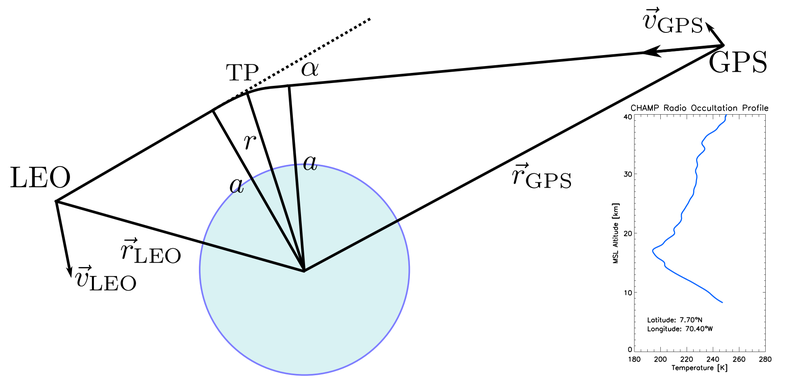

Figure 1: Geometry of an RO event. The GPS signal is refracted by the ionosphere and neutral atmosphere before it is received at a LEO satellite. Atmospheric parameters (like temperature, shown in the small panel) are derived from phase delay measurements.

BENDING ANGLE QUALITY

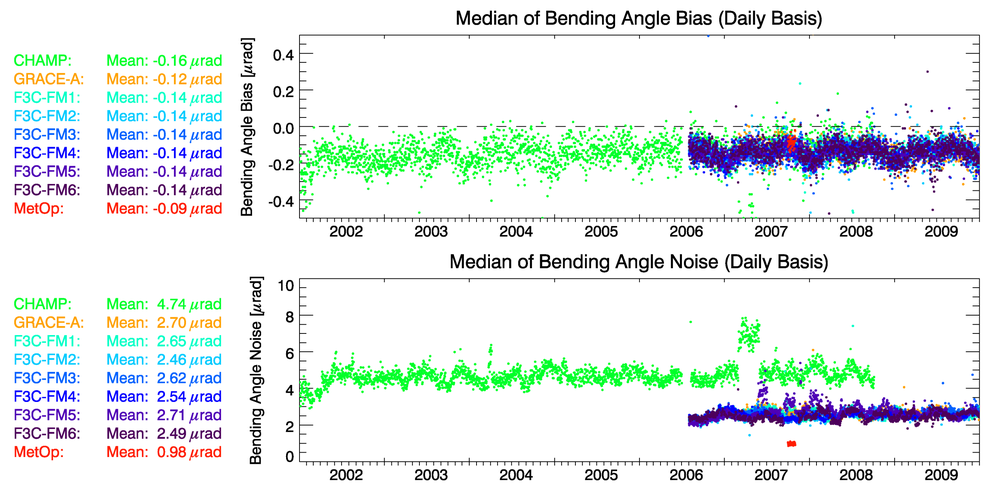

Figure 2: Temporal evolution of bending angle quality: Bending angle bias (top) and bending angle noise (bottom) from 2002 to 2009. Data are obtained from CHAMP (green), GRACE-A (yellow), F3C (6 satellites, blue), and MetOp/GRAS (red). Temporal mean values are shown on the left hand side of the panels.

The bending angle quality is estimated by comparing the ionosphere-corrected retrieved bending angle profile to its co-located MSIS profile between 65 km and 80 km. At these height levels, the measurement is dominated by measurement noise and ionospheric residuals because atmospheric density is small.
Figure 2 shows the temporal evolution of the bending angle bias (top) and the bending angle noise (bottom) from 2002 to 2009 for different satellites. The bending angle bias is slightly negative and very similar for all satellites. It seems that an annual cycle is superimposed on the bending angle bias because the bias is slightly larger during northern hemisphere winter than during northern hemisphere summer. While smallest bending angle noise is found for MetOp (0.98 μrad), it is largest for CHAMP (4.74 μrad). GRACE-A and F3C bending angle noise is similar and approximately 2.5 times larger than that of MetOp.

RO ERROR CHARACTERIZATION

RO error estimates are based on the comparison of retrieved RO profiles to co-located ECMWF reference profiles, giving the combined (RO observational plus ECMWF model) error. Figure 3 shows the global mean temperature bias and standard deviation for different RO satellites for the example month January 2008 (left panel) and for F3C/FM-1 for January 2007 to December 2009 (right panel). Below 35 km global data characteristics are very similar for all satellites and for all months.
The GPS RO observational error is determined by subtracting the estimated ECMWF error from the combined error in terms of variances. Since the estimated ECMWF error and the observational error are approximately of the same order of magnitude, a reasonable and simple estimate of the observed error can also be given by scaling the combined error with $1/\sqrt{2}$. Global error models are derived from fitting simple analytical functions to the GPS RO observational error. The observation error model s as function of altitude z is formulated as (cf. Steiner and Kirchengast 2005):

$$s(z) = \begin{cases} s_{\mathrm{UTLS}} + q_0 \left[\frac{1}{z^p} - \frac{1}{z_{\mathrm{TropTop}}^p} \right] & \text{for } 4 \text{ km} < z \le z_{\mathrm{TropTop}} \\ s_{\mathrm{UTLS}} & \text{for } z_{\mathrm{TropTop}} < z < z_{\mathrm{StratBot}} \\ s_{\mathrm{UTLS}} \cdot \exp\left(\frac{z - z_{\mathrm{StratBot}}}{H_{\mathrm{Strat}}(\lambda,d)} \right) & \text{for } z_{\mathrm{StratBot}} \le z < 35 \text{ km} \end{cases}$$

	z_{TropTop}	z_{StratBot}	s_{UTLS}	q_0	p	H_{Strat0}	$\Delta H_{\mathrm{Strat}}$
BA	14.0 km	22.0 km	0.8 %	10.0 %	1.0	18.0 km	5.0 km
N	14.0 km	20.0 km	0.35 %	2.5 %	1.0	15.0 km	5.0 km
p_{dry}	10.0 km	13.0 km	0.15 %	1.0 %	0.5	12.0 km	4.0 km
Z_{dry}	10.0 km	17.0 km	10.0 m	40.0 m	0.5	10.0 km	2.0 km
T_{dry}	10.0 km	20.0 km	0.7 K	5.0 K	0.5	15.0 km	8.0 km

where s_{UTLS} denotes the error in the UTLS domain, z_{TropTop} the top level of the troposphere domain, z_{StratTop} is the bottom level of the stratosphere domain, q_0 the best-fit parameter for the troposheric model, p the exponent, and H_{Strat} the scale height of the error increase over the lower stratosphere. H_{Strat} is modeled as a function of latitude λ and season d (sinusoidal seasonal variation with amplitude $\Delta H_{\mathrm{Strat}}$ at high latitudes beyond 60°, linearly decreasing to zero-amplitude within ±20° in the tropics). All parameters are modeled separately for BA, N, p_{dry}, Z_{dry}, T_{dry}.
Figure 4 shows the global observational error estimates and the global error model for all parameters except T_{dry}, Figure 5 depicts results for T_{dry} and for different latitude regions.

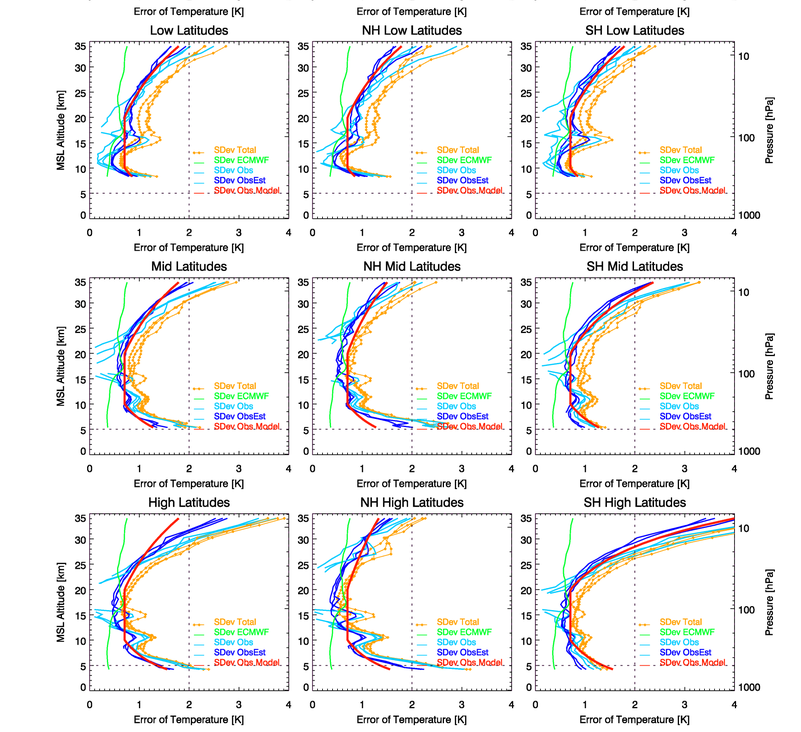

Figure 3: RO minus ECMWF temperature bias and standard deviation for all satellites in January 2008 (left panel) and for F3C/FM-1 from January 2007 to December 2009 (right panel).

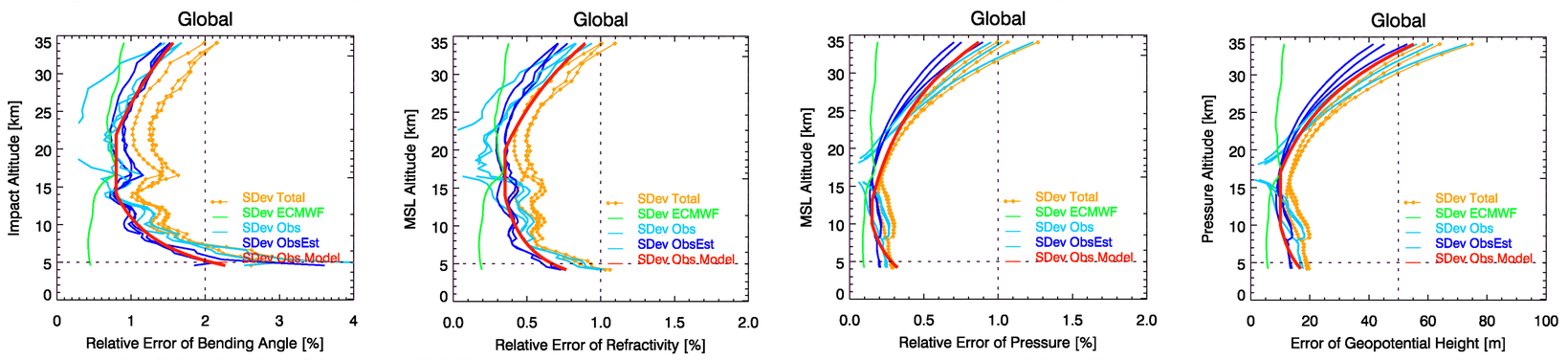

Figure 4: RO (CHAMP, GRACE-A, and F3C/FM-4) plus ECMWF combined error (yellow), estimated ECMWF error (green), observational error (light blue), estimated observational error (dark blue), and observational error model (red) in July 2008. Results are shown for bending angle, refractivity, dry pressure, and dry geopotential height (from left to right).

Figure 5: RO (CHAMP, GRACE-A, and F3C/FM-4) plus ECMWF combined error (yellow), estimated ECMWF error (green), observational error (light blue), estimated observational error (dark blue), and observational error model (red) in July 2008. Temperature (T_{dry}) results are shown for different latitude regions.

CONCLUSIONS

- Bending angle bias is slightly negative and very similar for all satellites.
- Even though the bending angle noise features strong satellite dependence, observational errors below 35 km are very similar for all satellites.
- Simple error modeling following Steiner and Kirchengast (2005) and Steiner et al., (2006) provides reasonable estimates of the observational error for GPS RO profiles of bending angle, refractivity, dry pressure, dry geopotential height, and dry temperature.

References

Steiner, A.K. and G. Kirchengast (2005), Error analysis of GNSS radio occultation data based on ensembles of profiles from end-to-end simulations, J. Geophys. Res., 110, D15307, doi:10.1029/2004JD005251

Steiner, A.K., A. Löscher, and G. Kirchengast (2006), Error characteristics of refractivity profiles retrieved from CHAMP radio occultation data, in Atmosphere and Climate: Studies by Occultation Methods (U. Foelsche, G. Kirchengast, A.K. Steiner, eds), Springer, Berlin-Heidelberg, 27-36